

The Munich Compact Light Source: initial performance measures

Elena Ettl,^{a,*} Martin Dierolf,^a Klaus Acherhold,^a Christoph Jud,^a
Benedikt Günther,^{a,b} Eva Braig,^a Bernhard Gleich^c and Franz Pfeiffer^{a,d}

Received 22 February 2016

Accepted 15 June 2016

Edited by A. Momose, Tohoku University, Japan

Keywords: inverse Compton X-rays; compact synchrotron; X-ray imaging.

^aPhysik-Department und Institut für Medizintechnik, Technische Universität München, James-Frank-Straße 1, 85748 Garching, Germany, ^bMax-Planck-Institut für Quantenoptik, Hans-Kopfermann-Straße 1, 85748 Garching, Germany, ^cInstitut für Medizintechnik, Technische Universität München, Boltzmannstraße 11, 85748 Garching, Germany, and ^dInstitut für Radiologie, Klinikum rechts der Isar, Technische Universität München, Ismaninger Straße 22, 81675 München, Germany. *Correspondence e-mail: elena.ettl@ph.tum.de

While large-scale synchrotron sources provide a highly brilliant monochromatic X-ray beam, these X-ray sources are expensive in terms of installation and maintenance, and require large amounts of space due to the size of storage rings for GeV electrons. On the other hand, laboratory X-ray tube sources can easily be implemented in laboratories or hospitals with comparatively little cost, but their performance features a lower brilliance and a polychromatic spectrum creates problems with beam hardening artifacts for imaging experiments. Over the last decade, compact synchrotron sources based on inverse Compton scattering have evolved as one of the most promising types of laboratory-scale X-ray sources: they provide a performance and brilliance that lie in between those of large-scale synchrotron sources and X-ray tube sources, with significantly reduced financial and spatial requirements. These sources produce X-rays through the collision of relativistic electrons with infrared laser photons. In this study, an analysis of the performance, such as X-ray flux, source size and spectra, of the first commercially sold compact light source, the Munich Compact Light Source, is presented.

1. Introduction

The Munich Compact Light Source (MuCLS) is the first commercially sold compact synchrotron source and has recently been installed at the Technische Universität München, Germany. The MuCLS was developed and manufactured by Lyncean Technologies Inc., USA. A compact synchrotron source, or compact light source (CLS), functions like a miniature synchrotron and produces a quasi-monochromatic X-ray beam with tunable X-ray energy, high flux and a large field of view. These characteristics and the currently available X-ray beam parameters make it perfectly suited for pre-clinical X-ray imaging of biomedical samples or for materials science research. The first concept has been published by Huang & Ruth (1998) and first imaging experiments have been published after more than ten years of development (Bech *et al.*, 2009). Previous experiments with a CLS showed the potential of the source for pre-clinical research, for example on the diagnosis of pulmonary emphysema (Schleede *et al.*, 2013) or breast cancer (Schleede *et al.*, 2012) and on the possibility to distinguish brown from white adipose tissue (Ettl *et al.*, 2015). Furthermore, Abendroth *et al.* (2010) demonstrated the feasibility of protein crystallography at a CLS.

Here, for the first time, we independently present and analyze data on the performance and characteristics of the



© 2016 International Union of Crystallography

X-ray beam of a CLS, such as produced spectra, beam shape, and stability of flux, source size and position, with the data acquired at the MuCLS, after initial installation and commissioning of the machine in Munich in April 2015.

2. The Compact Light Source

2.1. Principle of X-ray generation

The CLS is based on the concept of inverse Compton scattering, where X-rays are produced in the collision of a relativistic electron beam with a laser pulse. In the wave picture, this process can be regarded as X-rays being produced in a laser undulator, where the laser photons are seen as a counterpropagating electromagnetic wave by the electrons, in analogy to a permanent-magnet undulator at a synchrotron source. Importantly, the undulator period of the laser undulator is given by half the laser wavelength, *i.e.* about 0.5 μm, and therefore is about four orders of magnitude smaller than a permanent-magnet undulator period (~cm) (Huang & Ruth, 1998; Loewen, 2003). This allows for the electron energy to be reduced by the square root of this factor and hence also for the size of the electron storage ring to be scaled down to a few meters in circumference, making it possible for a CLS to fit into a standard laboratory. This facilitates the availability of nearly monochromatic X-rays and in principle enables the installation of a CLS at any research facility.

2.2. Technical realisation

Electrons are produced by a RF photocathode source where UV pulses¹ illuminate a Cu cathode to emit an electron bunch. The bunch is then accelerated to relativistic energies (25–45 MeV) in a linear accelerator section. They are injected into a miniature storage ring (~4.6 m circumference) by a kicker magnet, replacing the former electron bunch after about 2.6 million turns (25 Hz reinjection rate). Two laser pulses (1064 nm wavelength, Nd:YAG) are stored in a high-finesse bow-tie enhancement cavity (~9.2 m length), and are tightly focused at the interaction point, where X-rays are produced at each revolution of the electron bunch (Loewen, 2003), with a repetition rate of 64.91 MHz. The X-rays are emitted through a transmissive spot in the output mirror, where they are confined to a 4 mrad cone, and travel through an evacuated beam tube to the experimental setups.

2.3. X-ray beam characteristics

The X-ray energy is tunable and can be adjusted *via* the electron energy, since the laser wavelength is fixed. The X-ray energy in the process of inverse Compton scattering is given by

$$E_x = \frac{E_L(1 - \beta \cos \theta_i)}{(1 - \beta \cos \theta_f) + (E_L/E_e)[1 - \cos(\theta_f - \theta_i)]}, \quad (1)$$

¹ The laser is a frequency-quadrupled Nd:YLF laser with a wavelength of 262 nm. The repetition rate is 25 Hz with a pulse energy of ~120 μJ pulse⁻¹.

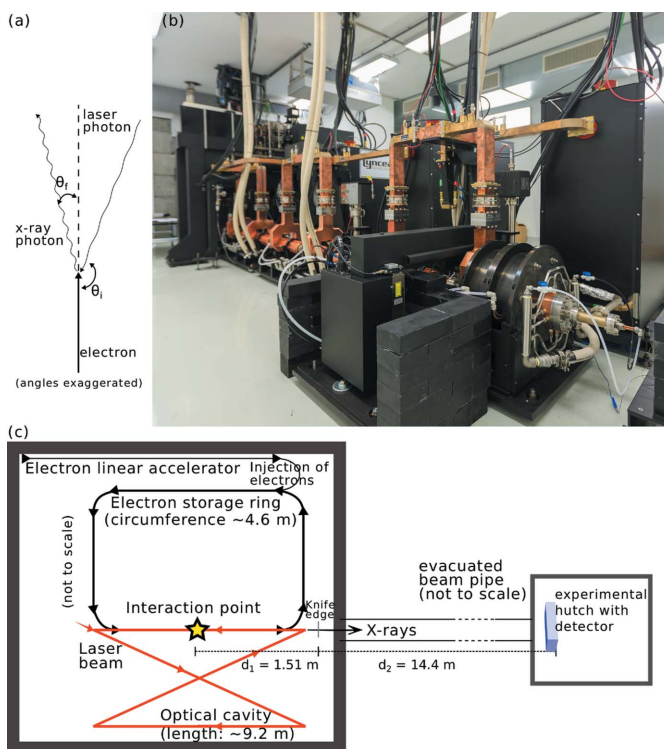


Figure 1
(a) Schematic representation of the process of inverse Compton scattering. (b) Photograph of the MuCLS. (c) Schematic drawing of the setup, not to scale.

where $\beta = v/c$, E_x is the X-ray energy, E_L is the laser photon energy, E_e is the electron energy, and θ_i and θ_f are incident and final scattering angles (Loewen, 2003). A schematic drawing of the scattering process is provided in Fig. 1(a). For head-on collision of laser and electron beam, and on-axis observation, the expression simplifies to

$$E_x = 4\gamma^2 E_L, \quad (2)$$

where $\gamma = E_e/E_0$, $E_0 = 511$ keV being the rest energy of an electron. Equation (2) provides a valid approximation for the X-ray energy, as the aperture of the output mirror confines the CLS beam to a 4 mrad cone, an angle considerably smaller than the full angular emission from the Compton process.

2.4. Installation of the MuCLS

The MuCLS is installed at the Institut für Medizintechnik of the Technische Universität München in Garching, Germany. The MuCLS is located inside a radiation shielding cave, which was built according to a patent from Forster Bau GmbH, Ingolstadt, Germany. The shielding walls have a sandwich-like construction, consisting of two 15 cm-thick walls of heavy concrete (2.3–4.0 tons m⁻³, depending on the location with respect to the bremsstrahlung emerging from the beam dump) and 50 cm of electric furnace slag in between (2.4 tons m⁻³, concrete with a weight portion of 23% iron).

From the radiation shielding cave, the X-rays travel through an evacuated beam pipe with Mylar windows to the experi-

mental setup, which is located in a radiation shielding hutch placed at a distance of approximately 15 m from the interaction point. A photograph of the MuCLS, showing mainly the accelerator section, and a schematic drawing of the full setup are shown in Figs. 1(b) and 1(c), respectively.

The total power consumption of the MuCLS is approximately 80 kW, of which the main part is required for cooling power.

3. X-ray beam shape

3.1. Results

A detector image of the full X-ray beam is shown in Fig. 2. The beam shape is almost round, with a divergence of approximately 4 mrad, with the vertical dimension slightly larger. At a distance of 16.61 m from the interaction point, the beam size (full width at half-maximum, FWHM) was 74.17 mm in the vertical dimension and 66.55 mm in the horizontal dimension, corresponding to divergences of 4.46 mrad and 4.01 mrad, respectively. Beam profiles show the flatness of the beam. The structure visible in the image is caused by the structure of the detector sensor.

3.2. Discussion

The shape and size of the X-ray beam are defined by the geometry of the X-ray transmissive spot of the output mirror of the laser cavity. The exit mirror is slightly tilted with respect to the axis of the X-ray beam, causing the football-like shape of the outcoming X-ray beam. As the X-ray energy decreases with increasing observation angle [*cf.* equation (1)], the spectrum of the X-ray beam will broaden with increasing beam size, *i.e.* there is a trade-off between beam size and monochromaticity. The chosen divergence angle of approxi-

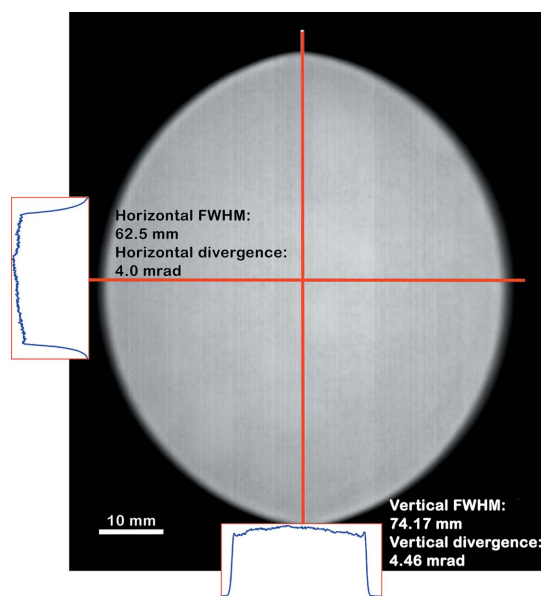


Figure 2
Detector image of the X-ray beam at 16.6 m distance from the interaction point taken with the Varian PaxScan, showing the divergence of approximately 4 mrad and the flatness of the beam.

Table 1

Peak energies and bandwidths of the measured spectra.

Peak energy (keV)	FWHM (keV)	Bandwidth $\Delta E/E$ (%)
15.26	0.46	2.99
24.78	0.89	3.60
34.96	1.50	4.29

mately 4 mrad is matched to the divergence angle of the electron beam and results in the best compromise between desirable large beam size and narrow bandwidth for our present application. The beam profiles show that the beam intensity is highly uniform across the profile, and sharply falls to zero at the cutoff, as the energy decrease with observation angle is very small in the chosen range.

4. X-ray spectra

4.1. Results

Spectra acquired for three different X-ray energies are presented in Fig. 3. Displayed are data for peak energies of 15.2 keV, 24.8 keV and 35.0 keV, normalized to their maximum value. In principle, the energy is freely tunable between 15 and 35 keV by adjusting the electron energy according to equation (2). All spectra show narrow peaks. The small peak visible for the 35.0 keV spectrum at 25 keV is due to the Sn- K_{α} fluorescence line of the solder of the thermoelectric cooler of the Amptek X-123 detector. The line at 28 keV is due to the Sn- K_{β} fluorescence.

The FWHM and bandwidths for the three measured spectra are given in Table 1, showing the quasi-monochromaticity of the source with a bandwidth $\Delta E/E$ of a few percent over the full energy range.

4.2. Discussion

The measured spectra show the narrow bandwidth of the MuCLS X-ray beam. From Fig. 3 it can be seen that the

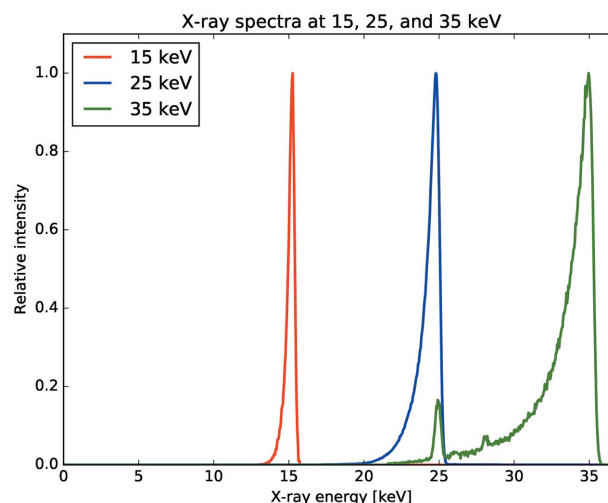


Figure 3
Measured spectra at peak energies of 15.2 keV, 24.8 keV and 35.0 keV.

spectra are broadened on both sides of the peak. While the high-energy tail is broadened by the electron energy spread $\Delta E_e/E_e$ and caused by distributions in electron energies and laser photon energies, the broadening of the low-energy tail mainly has its origin in the electron beam divergence $\Delta\theta_e$ (Loewen, 2003). The CLS spectrum widens with increasing X-ray energy [cf. equation (1)].

Previous studies (Achterhold *et al.*, 2013; Eggl *et al.*, 2015) have demonstrated that the quasi-monochromatic beam with a bandwidth of a few percent provided by the CLS is suitable for quantitative absorption imaging, allows beam hardening artifacts to be overcome, and enables a quantitative reconstruction of attenuation coefficient and refractive index decrement that is consistent with literature values.

5. X-ray beam properties and stability

5.1. Results

Over a duration of three hours with a frame rate of 1 Hz, we recorded the flux, the horizontal and vertical source sizes and the movement of the source, exemplarily shown for a peak X-ray energy of 24.8 keV. The time curves are displayed in Figs. 4, 5 and 6, respectively. Mean values for flux and source sizes and their standard deviations as well as the standard deviation for source movements are summarized in Table 2. The total integrated flux was mostly between 0.90×10^{10} and 1.05×10^{10} photons s^{-1} , with one short drop in flux about an hour into the run, yielding an average flux of 0.97×10^{10} photons s^{-1} with a r.m.s. deviation of less than 5%.

The r.m.s. source size is around 42 μm in both directions, with the horizontal size slightly larger and with a slightly higher standard deviation of 2% than for the vertical direction. The vertical source movement is also larger than the movement in the horizontal direction, but still small with a

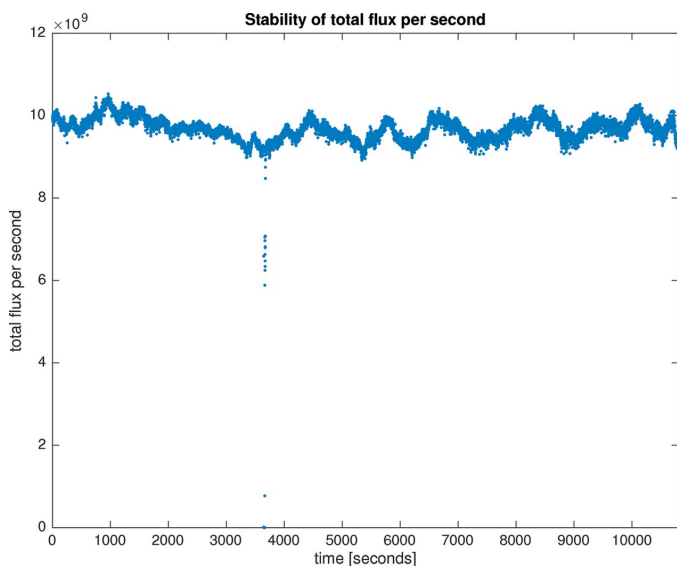


Figure 4 Time curve (10800 frames, 1 Hz) of the total flux (photons s^{-1}) measured with the Pilatus detector, after correction for detector efficiency and absorption in air and Mylar.

Table 2 Stability analysis of flux, source size and source position at a peak X-ray energy of 24.8 keV (values averaged over 3 h).

Quantity	Mean value	Standard deviation	Standard deviation (%)
Total flux (photons s^{-1})	9.654×10^9	0.478×10^9	4.95
Horizontal r.m.s. source size (μm)	41.5	0.4	1.0
Vertical r.m.s. source size (μm)	42.4	0.9	2.1
Horizontal source position [†] (μm)		1.5	
Vertical source position (μm)		3.9	

[†] Around average position.

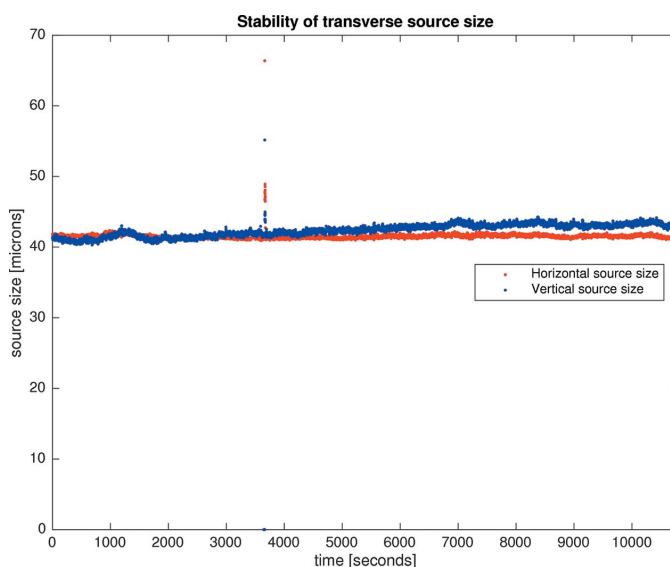


Figure 5 Time curve (10800 frames, 1 Hz) of horizontal and vertical source size, as derived from a fit of the error function to the knife-edge.

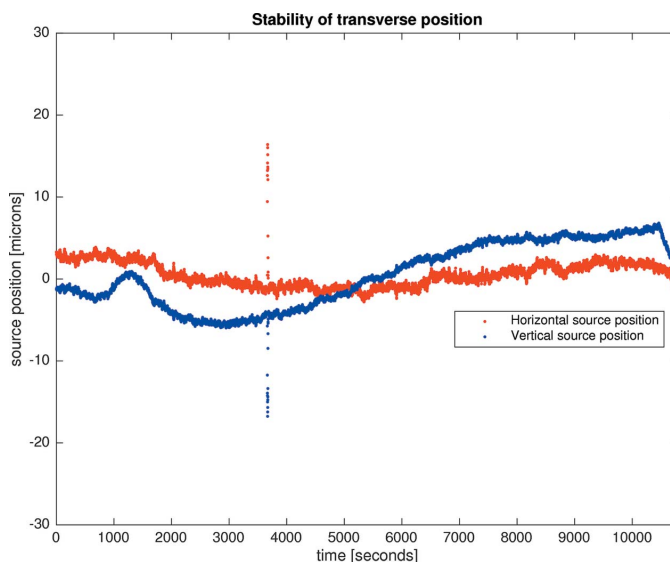


Figure 6 Time curve (10800 frames, 1 Hz) of the movement of the horizontal and vertical source position around the position mean.

Table 3

Typical operating values at a peak X-ray energy of 15.3 keV, 90 minutes after an energy change, averaged over 10 minutes.

Quantity	Mean value	Standard deviation	Standard deviation (%)
Total flux (photons s ⁻¹)	4.430 × 10 ⁹	0.050 × 10 ⁹	1.13
Horizontal r.m.s. source size (µm)	48.9	0.3	0.5
Vertical r.m.s. source size (µm)	44.0	0.9	2.1
Horizontal source position† (µm)		0.5	
Vertical source position (µm)		1.1	

† Around average position.

Table 4

Typical operating values at a peak X-ray energy of 35.0 keV, 90 minutes after an energy change, averaged over 10 minutes.

Quantity	Mean value	Standard deviation	Standard deviation (%)
Total flux (photons s ⁻¹)	1.78 × 10 ¹⁰	0.035 × 10 ¹⁰	1.83
Horizontal r.m.s. source size (µm)	41.7	0.3	0.8
Vertical r.m.s. source size (µm)	39.2	0.3	0.8
Horizontal source position† (µm)		0.5	
Vertical source position (µm)		0.3	

† Around average position.

standard deviation of less than 4 µm. The brilliance can be calculated from (Attwood, 1999)

$$B = \frac{\Phi \times 10^{-3}}{\Delta A \Delta \Omega (\Delta E/E) (0.1\% \text{ bandwidth})}, \quad (3)$$

where Φ is the total X-ray flux per second, $\Delta A = \pi\sigma^2$ is the source area, $\Delta \Omega \approx 4\pi\theta/4$ is the solid angle, and $\Delta E/E$ is the bandwidth of the spectrum. With the determined flux $\Phi \approx 1 \times 10^{10}$ photons s⁻¹, a bandwidth of $\Delta E/E = 0.03$, r.m.s. source size $\sigma \approx 42$ µm and r.m.s. angular spread $\theta = 4$ mrad, equation (3) gives a brilliance of $B = 4.8 \times 10^9$ photons s⁻¹ mm⁻² mrad⁻² (0.1% bandwidth)⁻¹ for an X-ray energy of 25 keV.

Concerning other X-ray energies, the flux roughly scales with the X-ray energy. Tables 3 and 4 present typical operating values for 15 keV and 35 keV peak energy, respectively. The data shown in these tables have been averaged over 10 min and were recorded 90 min after an energy change. The flux at 35 keV lies above the value expected from the energy scaling, while that for 15 keV is a bit lower, which is caused by the higher attenuation of low energies in the beryllium exit window of the CLS.

5.2. Discussion

The presented results show that the MuCLS produces stable flux over several hours and there is little variation in source size and position. This performance makes the source suitable for imaging experiments lasting several hours as demonstrated previously as well (Eggl *et al.*, 2015). The short drop in intensity around one hour into the run was caused as the laser cavity lost lock to the 64.91 MHz revolution frequency of the

storage ring, most likely due to an external influence, which was re-established immediately by the operators.

The typical operating values presented for two more energies show a similar behavior. Smaller source sizes and better flux can more easily be achieved for higher X-ray energies, as the electron beam becomes more stable at higher energies.

In order to improve the conditions for measurements even more, an X-ray beam intensity monitor and position monitor will be implemented in the future, so that the existence of an even higher stability throughout, for example, a tomography scan can be ensured.

6. Methods and materials

During the measurements, electrons with a charge of approximately 200 pC were stored, and the power stored in the laser cavity was approximately 70 kW.

The full X-ray beam was acquired in the experimental hutch using a Varian PaxScan 2520D flat panel detector with a CsI scintillator and a pixel size of 127 µm × 127 µm. The detector was located at a distance of 16.61 m from the interaction point. The divergence angle was calculated by dividing the FWHM of the beam by the distance from the interaction point.

The X-ray spectra were measured using an energy-dispersive Amptek X-123 detector. As an attenuator, 39 mm of PMMA were inserted for the 15 keV measurement and 78 mm of PMMA were inserted for the 25 keV and the 35 keV measurements. The Amptek detector was placed at a distance of 3.8 m from the interaction point. The energy channels were calibrated *via* the K_α and K_β lines from the fluorescence of a Cu plate. The measured spectra were corrected for the efficiency of the 500 µm-thick Si sensor of the Amptek detector and the transmission through PMMA. The bandwidth was calculated as the FWHM of the spectrum divided by the peak energy.

The X-ray stability scan was recorded at a peak X-ray energy of 24.8 keV using a Pilatus 100K (Dectris, Switzerland) detector with a pixel size of 172 µm × 172 µm and a 1000 µm Si sensor. The detector was located at 15.91 m from the interaction point. A knife-edge was placed at a distance of 1.51 m from the interaction point. This resulted in a magnification of 9.54. We recorded 10800 frames with an exposure time of 0.99 s and a read-out time of 0.01 s, corresponding to a total scan time of three hours. The X-ray flux was calculated from a region of interest (ROI) of 50 × 50 pixels by multiplying the average flux per pixel by the number of pixels covered by the full beam. The flux was corrected for the absorption of the X-rays in air gaps (870 mm) and Mylar foils (0.5 mm), as well as the efficiency of the sensor of the detector. The transmission and effectivity values were calculated using tabulated data from the XMuDat database (R. Nowotny, Institut für Biomed. Technik und Physik, Universität Wien, Austria) taking into account the measured spectrum at 24.8 keV. The r.m.s. source size and the source movement were calculated averaging 50 pixel lines along the horizontal and the vertical edge of the knife-edge, respectively. We ensured that the edge was not tilted with respect to the pixels. The

point spread function (one pixel wide, box-shaped) of the Pilatus detector was taken into account when fitting an error function,

$$f(x) = a \operatorname{erf}\left(\frac{x-b}{\sqrt{2}c}\right) + d, \quad (4)$$

to the knife-edge. The r.m.s. source size then is given by the standard deviation c , and b indicates the relative source position. The fit was performed with the *fit* function using a Levenberg–Marquardt algorithm implemented in Matlab. The ROIs used for calculating flux and source parameters are displayed in an exemplary detector image shown in Fig. 7, where F indicates the ROI used for the flux calculation, and H and V indicate the ROIs used for horizontal and vertical parameters, respectively.

7. Conclusion and outlook

We have presented data on the performance of the Munich Compact Light Source, a compact laser-driven synchrotron source, after initial installation in Munich in April 2015. The data show that the machine produces a stable X-ray beam with a flux of about 10^{10} photons s^{-1} and source sizes of about $42 \mu\text{m}$ in both transverse directions. With an r.m.s. variation of

less than 5% of the flux and 1–2% of source sizes over three hours, the X-ray beam provides sufficient stability also for long X-ray imaging experiments, such as grating-based tomographic imaging. Typical operating values for energies of 15 keV and 35 keV show a similar behavior at these energies. Compared with previously published X-ray imaging studies (Eggl *et al.*, 2015), scans can be acquired significantly faster thanks to the flux having increased by about a factor of three in the meantime.

In the near future, we will develop the experimental infrastructure for a fully functional imaging beamline at MuCLS for biomedical and material science applications. Furthermore, efforts will be made to further improve the X-ray flux, a task that can be accomplished for example by increasing stored power in the laser cavity, storing electron bunches of higher charge or by advances in cavity mirror design. The stability of the MuCLS is expected to improve by implementation of even more sophisticated feedback systems.

Overall, the presented evidence shows that the CLS technology has evolved far enough to provide suitable conditions for X-ray imaging with a quasi-monochromatic beam produced by a laboratory-scale device.

Acknowledgements

The authors acknowledge financial support through the DFG Cluster of Excellence Munich-Centre for Advanced Photonics (MAP), the Center for Advanced Laser Applications (CALA), the German Federal Ministry of Education and Research (BMBF), the DFG Gottfried Wilhelm Leibniz program and the European Research Council (ERC, FP7, StG 240142).

References

Abendroth, J., McCormick, M. S., Edwards, T. E., Staker, B., Loewen, R., Gifford, M., Rifkin, J., Mayer, C., Guo, W., Zhang, Y., Myler, P., Kelley, A., Analau, E., Hewitt, S. N., Napuli, A. J., Kuhn, P., Ruth, R. D. & Stewart, L. J. (2010). *J. Struct. Funct. Genomics*, **11**, 91–100.

Achterhold, K., Bech, M., Schleede, S., Potdevin, G., Ruth, R., Loewen, R. & Pfeiffer, F. (2013). *Sci. Rep.* **3**, 1313.

Attwood, D. (1999). *Soft X-rays and Extreme Ultraviolet Radiation: Principles and Applications*, pp. 165–168. Cambridge University Press.

Bech, M., Bunk, O., David, C., Ruth, R., Rifkin, J., Loewen, R., Feidenhans'l, R. & Pfeiffer, F. (2009). *J. Synchrotron Rad.* **16**, 43–47.

Eggl, E., Schleede, S., Bech, M., Achterhold, K., Loewen, R., Ruth, R. D. & Pfeiffer, F. (2015). *Proc. Natl Acad. Sci. USA*, **112**, 5567–5572.

Huang, Z. & Ruth, R. D. (1998). *Phys. Rev. Lett.* **80**, 976–979.

Loewen, R. (2003). *A Compact Light Source: Design and Technical Feasibility Study of a Laser–Electron Storage Ring X-ray Source*, SLAC Report 632. Stanford University, USA.

Schleede, S., Bech, M., Achterhold, K., Potdevin, G., Gifford, M., Loewen, R., Limborg, C., Ruth, R. & Pfeiffer, F. (2012). *J. Synchrotron Rad.* **19**, 525–529.

Schleede, S., Meinel, F. G., Bech, M., Herzen, J., Achterhold, K., Potdevin, G., Malecki, A., Adam-Neumair, S., Thieme, S. F., Bamberg, F., Nikolaou, K., Bohla, A., Yildirim, A. Ö., Loewen, R., Gifford, M., Ruth, R., Eickelberg, O., Reiser, M. & Pfeiffer, F. (2013). *Proc. Natl Acad. Sci. USA*, **109**, 17880–17885.

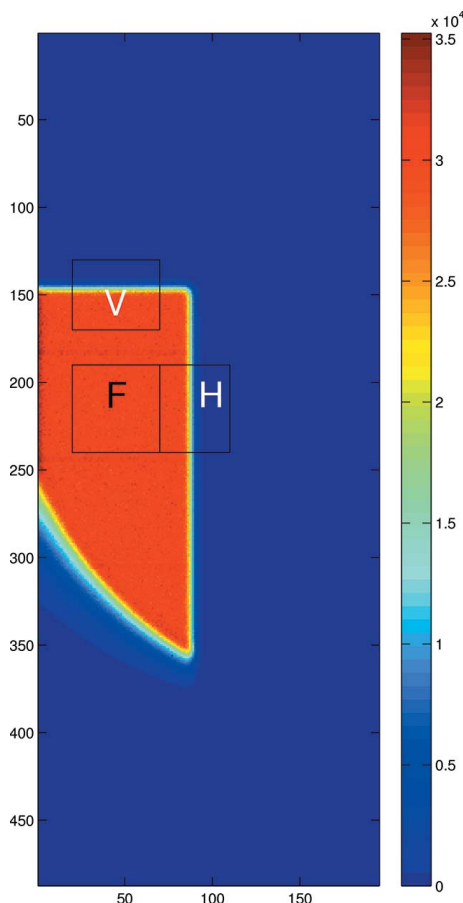


Figure 7 Exemplary detector image taken with the Pilatus 100K detector for the stability analysis. The rectangles indicate the ROIs used for calculation of flux (F), horizontal (H) and vertical (V) parameters.